Resonant Frequencies in Aviation Platforms

by

Robert Jarrett Branch

A thesis submitted to the Graduate Faculty of
Auburn University
in partial fulfillment of the
requirements for the Degree of
Master of Science

Auburn, Alabama
May 10, 2015

Keywords: electromagnetic, waveguide
resonance,

Approved by

Thomas Shumpert, Chair, Professor Emeritus of Electrical Engineering
Lloyd Riggs, Professor of Electrical Engineering
Michael Baginski, Associate Professor of Electrical Engineering

Abstract

This thesis examines the coupling effects of electromagnetic fields to the interior of aviation platforms during electromagnetic vulnerability (EMV) testing and the potential of resonant frequency field enhancements. Interior fields of a cylindrical slotted cylinder (approximate half scale model representation of the Black Hawk helicopter) were measured with and without the presence of a ground plane. Maximum permissible exposure (MPE) limits are presented as well as MPE measurements interior to different helicopter platforms. Lastly, the effects these measured fields have on testing are examined.

Acknowledgements

The author would like to thank his committee chair, Dr. Thomas Shumpert, for his assistance and guidance throughout the Master of Science program. This thesis would not have been possible without his direction and knowledge of the subject matter. I would also like to thank the Electromagnetic Environmental Effects test division of Redstone Test Center for their measurements and for providing the equipment and resources needed to complete this project. Lastly, thanks go to all the family members, friends, coworkers and professors for their support during this process.

Table of Contents

List of Tables

List of Figures

CHAPTER 1

INTRODUCTION

1.1 Background and Motivation

Electromagnetic Vulnerability (EMV) testing of Army rotary wing aircraft requires extremely high amplitude (peak and rms) electromagnetic (EM) fields to be generated. These levels are defined in Aeronautical Design Standard ADS-37A-PRF "Electromagnetic Environmental (E^3) Performance and Verification Requirements". Per requirements it is necessary to expose functional military systems to EM environments that it will encounter in the field. The system under test must meet its operational performance requirements when subjected to the radiated EM fields. The presence of personnel inside the aircraft is required to verify the operability of the system when these fields are present. Consequently, it is important to understand the internal fields present. As a safety requirement, the internal fields at the positions where aircraft personnel will be located must be measured prior to the start of testing. Maximum Permissible Exposure (MPE) limits are specified in IEEE Standard C95.1a-2010 "Standard for Safety Levels with Respect to Human Exposure to Radio Frequency Electromagnetic Fields". Field amplitudes that exceed the safety levels defined within this document require a reduction in either the radiating power or test time that personnel are exposed to the excessive field levels. Since Department of Defense (DoD) Interface Standard MIL-STD-464C "Electromagnetic Environmental Effects Requirements for Systems" and ADS-37A-PRF dictate the field requirements, test time is typically reduced due to the high field levels.

1.2 Outline

This thesis will focus on resonant frequencies, specifically cylindrical cavities and how these cavities affect the electromagnetic fields in the aircraft. Chapter 2 provides a general discussion of cylindrical cavities, with the support of theory and formulas to illustrate how these effects can be problematic when testing to such high field levels. Transverse Electric (TE) and Transverse Magnetic (TM) modes are taken into consideration. Measurements have been performed at Redstone Test Center on a slotted cylinder in an anechoic chamber with the presence of a conducting ground plane and without the ground plane. These measurements are compared to models developed by Shumpert, ETAL [2]. Next, Chapter 3 discusses the field level requirements of EMV testing of Army aircraft and provides data that was taken during MPE measurements on several different platforms. The primary focus is on the Boeing CH-47 Chinook helicopter. Data from the Boeing AH-64 Apache and Sikorsky UH-60 Black Hawk is included. Measurements recorded in the cockpit and crew areas of the CH-47 are analyzed.

CHAPTER 2

RESONANT FREQUENCIES

2.1 Introduction

This section examines the benefits of waveguides and the use of resonant frequencies to obtain high electromagnetic fields with minimal power. The advantages and applications of waveguides are discussed, as well as their modes of operations. Lastly, experimental data is used to confirm the presence of resonant frequencies measured inside various structures.

2.2 Waveguides

The propagation of electromagnetic waves can be accomplished with the use of a waveguide. Waveguides are used in a variety of applications to carry electromagnetic energy from one point to another. The capability of guiding high powered electromagnetic fields with very minimal loss is a major advantage of using a waveguide. In this thesis, the primary focus will be on a hollow waveguide, and particularly a hollow circular waveguide.

2.3 Advantage of Waveguides

Waveguides have two major advantages over other transmission lines. Waveguides have the capability to handle extremely high power fields with very little loss. Coaxial transmission lines are significantly impacted by the surface area of the current carrying inner conductor. The magnitude of the field is limited by the size of the center conductor. Skin effect reduces the size of the center conductor and causes the coax to be even less efficient. Secondly, the dielectric loss is much lower in waveguides as compared to a coaxial cable. In a coax, the dielectric loss is

caused by the heating of the insulation between the two conductors. The dielectric in a waveguide is air. Lastly, the power handling capability of a transmission line is directly related to the distance between conductors, consequently waveguides have the ability to handle more power given both are of the same size.

2.4 Circular Waveguides

A waveguide supports both transverse electric (TE) and transverse magnetic (TM) waves. Transverse electromagnetic (TEM) waves are differentiated by the absence of longitudinal field components. For that reason, TE modes have no electric field in the direction of propagation; likewise, TM modes have no magnetic field in the direction of propagation.

2.4.1 TE Modes

The propagation constant of the TEnm mode of a circular waveguide with an inner radius a is

$$\beta_{nm} = \sqrt{k^2 - k_c^2} = \sqrt{k^2 - \left(\frac{p'_{nm}}{a}\right)^2}$$

where $= \omega\sqrt{\mu\epsilon}$, with a cutoff frequency of

$$f_{c_{nm}} = \frac{k_c}{2\pi\sqrt{\mu\epsilon}} = \frac{p'_{nm}}{2\pi a\sqrt{\mu\epsilon}}.$$

Table 2.1. Values of p'_{nm} for TE Modes of a Circular Waveguide

N	p'_{n1}	p'_{n2}	p'_{n3}
0	3.832	7.016	10.174
1	1.841	5.331	8.536
2	3.054	6.706	9.97

The first TE mode to propagate is the mode with the smallest p'_{nm}, which is the TE_{11} mode, where p'_{11} =1.841.

2.4.2 TM Modes

The propagation constant of the TM_{nm} mode of a circular waveguide with an inner radius a is

$$\beta_{nm} = \sqrt{k^2 - k_c^2} = \sqrt{k^2 - \left(\frac{p_{nm}}{a}\right)^2}$$

with a cutoff frequency of

$$f_{c_{nm}} = \frac{k_c}{2\pi\sqrt{\mu\epsilon}} = \frac{p_{nm}}{2\pi a\sqrt{\mu\epsilon}}.$$

Table 2.2. Values of p_{nm} for TM Modes of a Circular Waveguide

N	p_{n1}	p_{n2}	p_{n3}
0	2.405	5.52	8.654
1	3.832	7.016	10.174
2	5.135	8.417	11.62

The first TM mode to propagate is the TM_{01} mode, where $p_{01} = 2.405$. p'_{11} is smaller than p_{01}.

As a result, the TE_{11} mode is the dominate mode of the circular waveguide.

2.4.3 Cylindrical Cavities

The resonant frequency of the TE_{nml} mode is

$$f_{nml} = \frac{c}{2\pi\sqrt{\mu_r\epsilon_r}}\sqrt{\left(\frac{p'_{nm}}{a}\right)^2 + \left(\frac{l\pi}{d}\right)^2}.$$

The resonant frequency of the TM_{nml} mode is

$$f_{nml} = \frac{c}{2\pi\sqrt{\mu_r\epsilon_r}}\sqrt{\left(\frac{p_{nm}}{a}\right)^2 + \left(\frac{l\pi}{d}\right)^2}.$$

The dominant TE mode is the TE_{111} mode, while the dominant TM mode is the TM_{110} mode.

2.5 Experimental Data

The experiments discussed in this section were performed at RTC. It is important to understand fields internal to aviation platforms due to RTC test requirements. The first experiment was performed in an anechoic chamber. Internal fields of a slotted circular cylinder were measured with and without the presence of a ground. The second experiment measured fields internal to a Cobra helicopter shell. These controlled experiments only strengthened the need to measure internal fields due to test environments prior to testing.

2.5.1 Slotted Circular Cylinder

Due to the nature of the testing performed at RTC, specifically EMV and EMRO testing, the coupling of fields into ground vehicles and aircraft is of great interest. RTC personnel conducted an experiment to better understand the potential of fields coupling into aircraft. They measured the fields coupled into a slotted cylinder from radiating sources at different antenna distances. Figure 2.1 shows the measurement setup. Measurements were taken with (Figures 2.4 and 2.5) and without (Figures 2.2 and 2.3) the presence of a ground plane. The cylinder was designed to be a half scale model representation of the Blackhawk helicopter. The cylinder was 7.62 m (25 ft) in total length with a diameter of 1.219 m (4 ft). The cylinder consisted of an axial slot with an aperture angle of 20 degrees. The slot had physical dimensions of approximately 0.2128 m (8 3/8 in) in width and 7.62 m (25 ft) in length along the cylinder. The cylinder was positioned broadside the radiating source, which can be seen in the figure below. The radiating source was always positioned with the source "shining" directly into the slot. Measurements were taken at 13 specific locations inside the cylinder using electric field probes.

Figure 2.1. Measurement Test Setup.

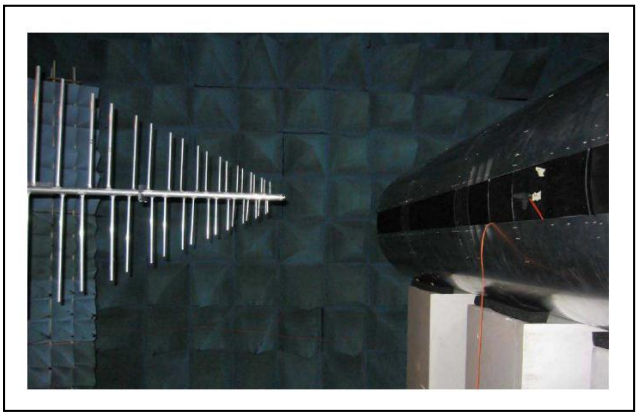

Measurements were first taken inside an anechoic chamber with floor treatment. Anechoic pyramids were positioned to create an environment without the presence of a ground plane. Three different antenna types (biconical dipole, LPDA, and ridged horn) were used as radiating sources. Measurements were taken as far away as possible within the confines of the anechoic chamber. The biconical and rigid horn were positioned 7 m away, while the LPDA was positioned 5 m away. Comparing the results from these three different radiating sources confirmed that the electric field had little dependence on the actual geometry or type of radiating source. It was decided to use the LPDA as the primary radiating source for all additional measurements because it best covered the frequency range of interest. Prior to the measurements, free field calibrations using the LPDA were made with an applied field of 20 V/m at a distance of 5 m with the cylinder not present. The cylinder was then moved into place and measurements were taken. Measurements of the fields in the aperture of the slot over a frequency range of 100 MHz to 400 MHz (in 2 MHz steps) were measured and compared to modeled data. Electric field amplitudes for both the TE and TM polarizations were recorded. The TE polarization is defined to be the orientation of the source antenna when the electric field is transverse to the longitudinal axis of the cylinder. For this experiment, the electric field of the source antenna was vertical. For the TM polarization the electric field of the source was horizontal. Figures 2.2 and 2.3 show the

spatially average fields that were measured inside the cylinder (with floor treatment). The spatial average was done in a manner that is consistent with calculations performed for MPE levels. The composite electric field amplitude at each of the 13 unique, interior positions is squared, summed and the square root of this resulting sum represents the spatially average electric field in the interior of the cylinder.

Figure 2.2. "Spatially Averaged" Internal Fields, Vertical/TE.

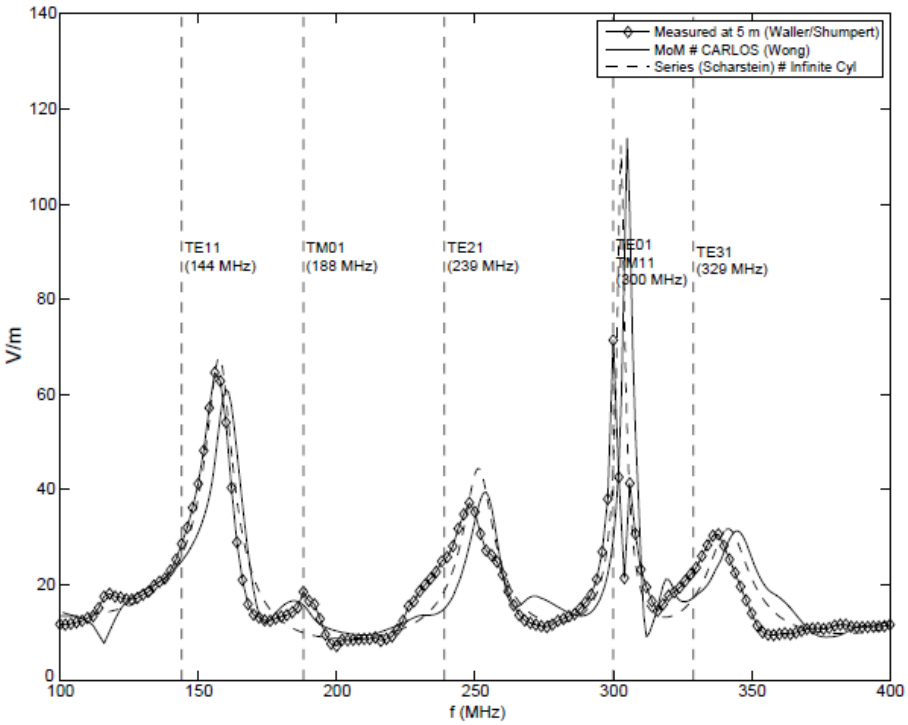

Figure 2.3. "Spatially Averaged" Internal Fields, Horizontal/TM.

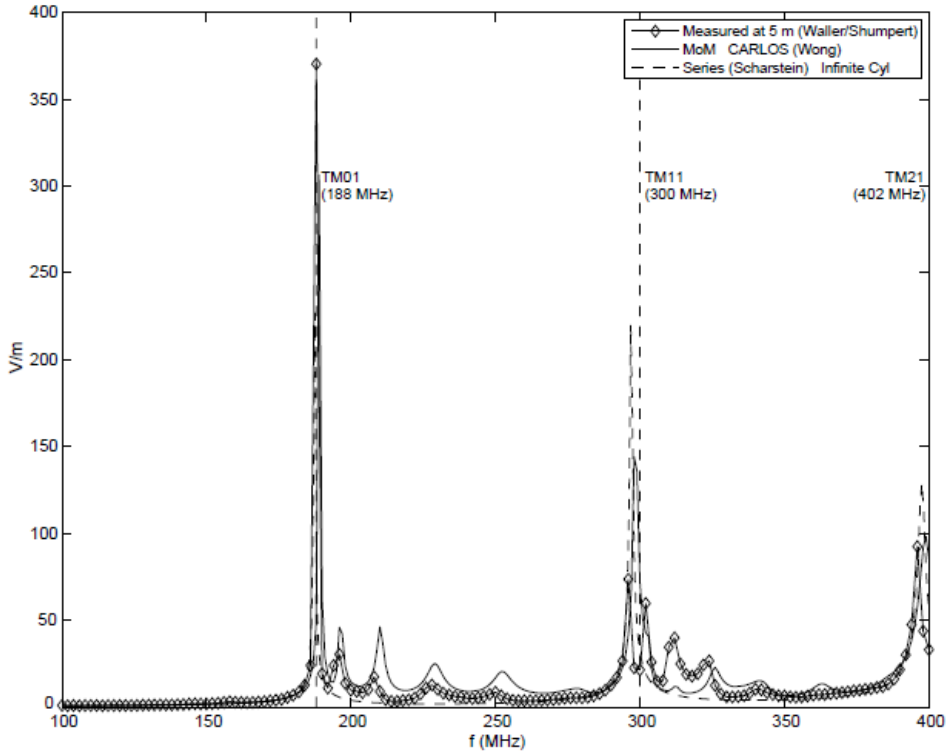

Those measurements are compared with an infinite series solution (dashed curve) for the fields in the infinite axial slot with two-dimensional infinite length cylinder and a three-dimensional moment method code (solid curve) for the finite perfect electric conductor cylinder with an axial slot running the length of the cylinder. The correlation between the measured and modeled data was very encouraging, specifically the amplitudes. As expected, the cylindrical modes for the TE cases are TE11-144 MHz, TE21-239 MHz, TE01-300 MHz, and TE31-329 MHz. The TM cases are TM01-188 MHz, TM11-300 MHz, and TM21-402 MHz. The modes are labeled and indentified with vertical dashed lines. It can be seen that there are enhancements at several frequencies within the selected frequency range. The enhancements are as high as 350% for the TE case at specific resonant frequencies and exceeds 1500% for the TM case.

Further measurements were then made with a ground plane present. The anechoic material was moved and replaced with an aluminum ground plane. To determine the effect of the inserted ground plane, measurements were made at varying heights from the cylinder axis to the ground plane (0.940 m, 1.295 m, and 2.515 m). Once again, the LPDA was used as the source antenna at a distance of 5 m away. The LPDA was radiating at a height that was equal to that of the cylinder axis. Figures 2.4 and 2.5 represent the spatially average of the electrical fields measured inside the hollow cylinder with the presence of a ground plane (aluminum floor treatment). The applied free field radiated by the LPDA was again 20 V/m.

Figure 2.4. Internal Fields, Vertical/TE.

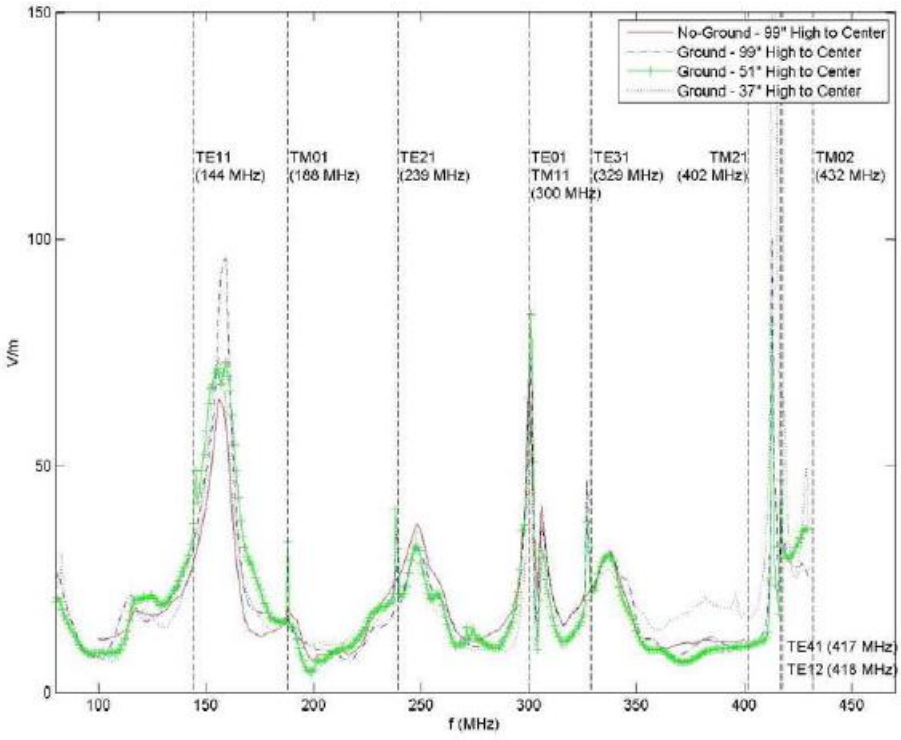

Figure 2.5. Internal Fields, Horizontal/TM.

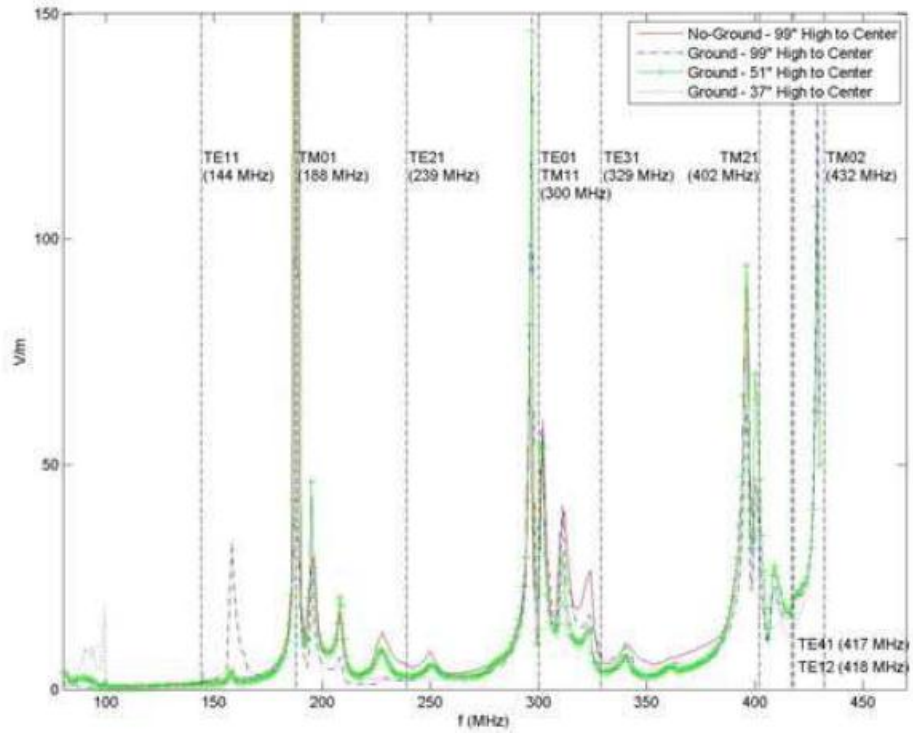

The presence of the ground plane did not result in order of magnitude changes to the overall responses seen except at very few specific frequencies.

In effect, all modes excited in the case with no ground plane present are also excited when the ground plane is present regardless of the height of the cylinder above the ground plane. For both cases it is seen that the interior fields inside the cylinder can be significantly greater than the field applied. This data has a direct relevance to EMV testing of helicopters and will be discussed in greater detail in Chapter 3.

2.5.2 Cobra Shell Helicopter Measurements

EM field measurements were made inside the cockpit of a Bell AH-1 Cobra helicopter by Redstone Test Center E3 personnel. For this experiment the EM field was calibrated to 20 V/m in open space as was done in the slotted cylinder experiment. The test item, Cobra helicopter, was then moved into place and measurements were taken in the front seat of the cockpit, head

and abdomen locations. The radiating source or transmitting antenna was placed at 5 different test positions around the cockpit of the helicopter as shown in the figure below. Discrete test frequencies ranged from 54 MHz to 2.6 GHz. Measurements were taken for both horizontal and vertical polarizations.

Figure 2.6. Radiating Positions

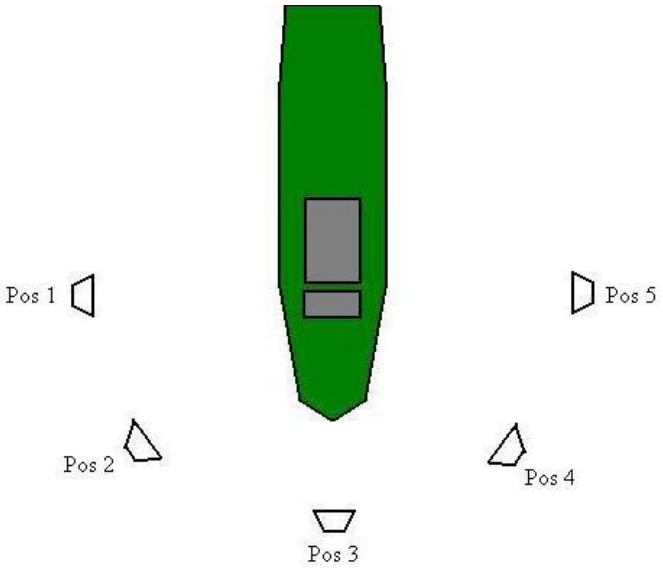

It can be seen in the figures below that the measured fields often times were in excess of twice the calibrated field. These cavity effects can greatly reduce the allowable test time during EMV testing due to personnel being in the field.

Figure 2.7. Cobra Cockpit E-Field Levels (Horizontal Polarization)

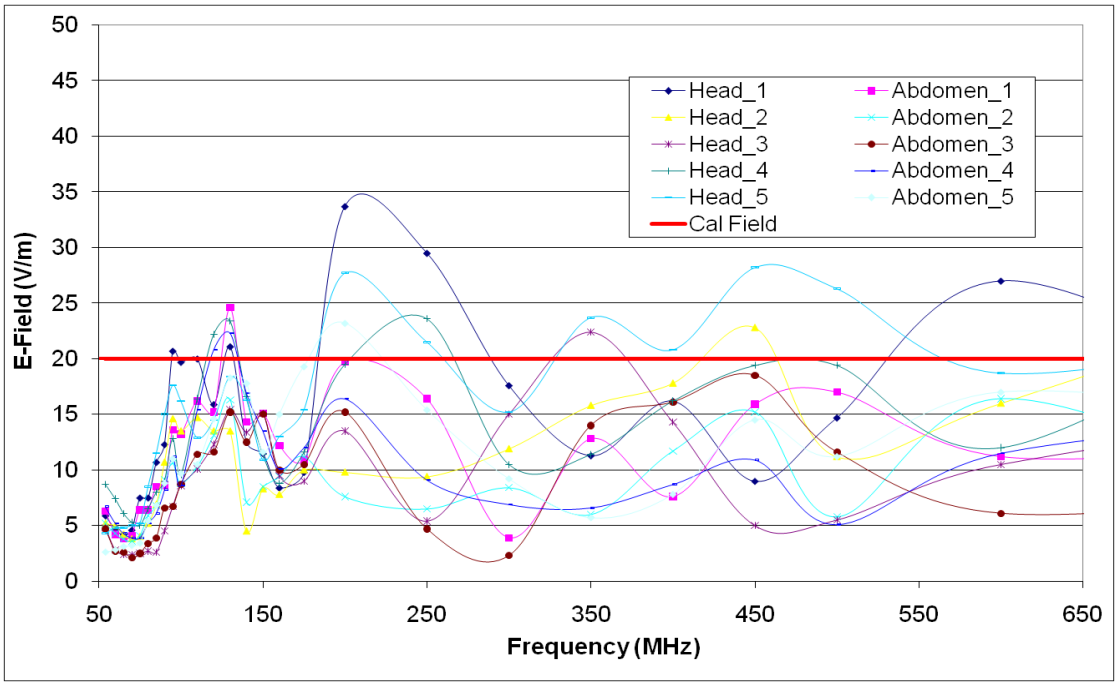

Figure 2.8. Cobra Cockpit E-Field Levels (Vertical Polarization)

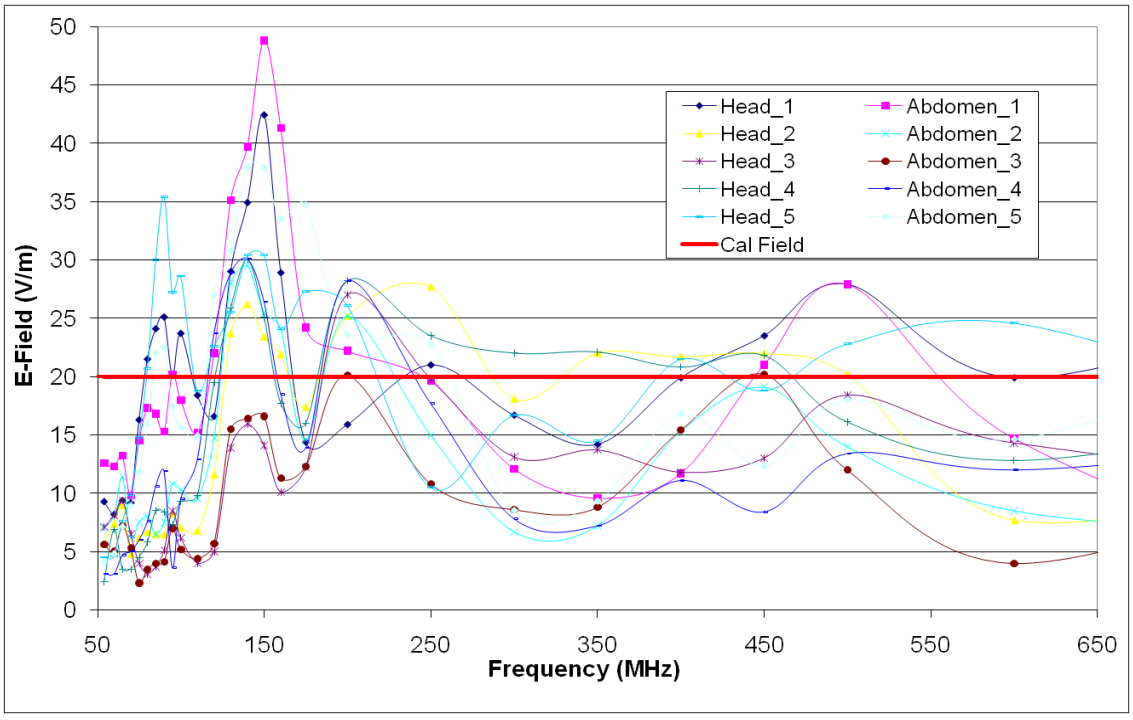

These measurements and model predictions confirm that internal cavity resonances can produce internal E-field values that significantly exceed the applied E-field values (i.e., the calibrated values produced when the cylinder "modeled helicopter" is not there.) In the next

chapter, measurements of the actual E-fields measured inside "real" helicopters are compared to the calibrated (applied) E-fields used in EMV testing. The comparison of these E-field values are discussed, the implications for safely testing aircraft to high-level EMV fields are identified.

CHAPTER 3

MEASURED INTERNAL ELECTROMAGNETIC FIELDS

3.1 Introduction

Army systems and subsystems must not be susceptible when exposed to external electromagnetic environments. Systems are required to meet operational requirements while in the presence of electromagnetic environments caused by either external sources or onboard transmitters. There are two primary documents that define the test fields for Army aviation systems and rotary wing aircraft. Those documents are MIL-STD-464C "Department of Defense Interface Standard: Electromagnetic Environmental Effects Requirements for Systems" and ADS-37A-PRF "Aeronautical Design Standard: Electromagnetic Effects (E^3) Performance and Verification Requirements".

3.2 Mil Standards

The maximum external electromagnetic environments for rotary wing aircraft found within MIL-STD-464C have been modified by the Aviation Engineering Directorate (AED) to better represent the world-wide environments that aviation systems may encounter. Table 3.1 defines the environments external to the aircraft, excluding the pulse parameters. Table 3.1 is broken down into frequency ranges. Each frequency range has an associated modulation(s), average electric field strength and sample size. Ideally, during EMV testing, systems or test articles would be immersed in the full spectrum of each of these ranges. However, due to test duration restrictions, discrete sample frequencies within each range are chosen. If a range lists

both CW and AM, both modulations will be tested as separate field environments. Additionally, both vertical and horizontal polarizations are required for each environment; only the vertical polarization is tested below 30 MHz. Each discrete frequency, along with a specific modulation, polarization, and field strength make up a single test environment.

Table 3.1: ADS-37A-PRF STANDARD WORLD-WIDE ELECTROMAGNETIC ENVIRONMENT (EXTERNAL TO AIRCRAFT) MODULATION PARAMETERS (EXCLUDING PULSE)

Frequency Range (MHz)		Mod	Electric Field (V/m - rms)	Sample Frequencies
			Average	
0.014	1.99	CW, AM	200	Continuous Sweep
2	19.9	CW, AM	200	Continuous Sweep
20	149.9	CW, AM, FM	200	Continuous Sweep
150	249.9	AM, FM	200	Continuous Sweep
250	499.9	AM, FM	200	Continuous Sweep
500	999.9	AM, FM	200	Continuous Sweep
1000	1999.9	AM, FM	200	Continuous Sweep
2000	3999.9	AM, FM	200	Continuous Sweep
4000	7999.9	AM, FM	200	Continuous Sweep
8000	9999.9	AM, FM	200	Continuous Sweep
10000	40000	CW, FM	200	Continuous Sweep

For the FM modulation, below 1 GHz uses a 20 kHz deviation modulated by a 1 kHz tone; above 1 GHz a 1 MHz deviation modulated by a 10 kHz square wave is used. The AM modulation is modulated by 1000 Hz tone with 50% modulation.

Table 3.2 defines the pulse environments. Again, the pulse modulation (PM) table is broken down into frequency ranges. Now each frequency range has a peak and average field strength, as well as a pulse width (PW) and a pulse repetition frequency (PRF). The sample size specifies how many discrete frequencies that are required to be tested for each frequency range. Both vertical and horizontal polarizations will be tested, expect below 30 MHz is vertical only.

Table 3.2: ADS-37A-PRF PULSE MODULATION PARAMETERS

Frequency Range (MHz)		Electric Field (V/m - rms)		PW (usec)	PRF (Hz)	Sample Frequencies
		Peak	Average			
2	24.9	204	102	833.3	300	24
150	249	3120	200	20-25	200-310	4
250	499.9	2830	200	25-33	300	6
500	999.9	3480	244	33	100-300	3
1000	1999.9	8420	200	1-2	670-1000	1
2000	3999.9	21270	336	1	250-600	3
4000	7999.9	21270	336	1-2	250	1
8000	9999.9	21270	336	1	150-250	2
10000	40000	6892	200	1	1000	6

3.3 Calibration

The electromagnetic environments defined in Tables 3.1 and 3.2 are calibrated prior to the EMV test. Calibrations are performed free-field, open air, without the test item or helicopter present. Figure 3.1 shows a typical calibration setup for a continuous wave (CW) signal. The electric field produced from the PM environments are measured using a receive antenna in place of the electric field probe. For the purpose of this chapter only the CW or average field environments are of interest. A calibration is performed for every unique field environment. The separation distance of the transmit antenna or radiating source is maximized to ensure EUT is within the radiating antenna's 3 dB beamwidth, but small enough to still obtain the required field levels.

Figure 3.1. Calibration Setup

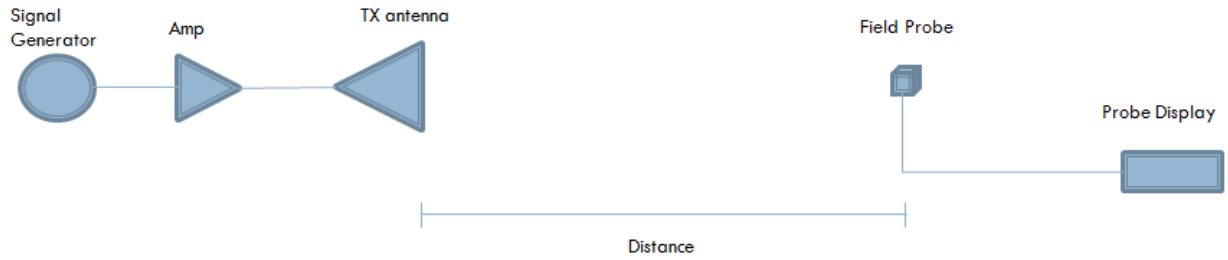

An electric field probe is positioned at the intended test separation distance. The equipment settings (distance, power level, etc) are recorded for each field environment. After calibrations are performed for each test environment, the helicopter or test item is then moved into place. However, to ensure the safety of personnel, the field strengths where personnel will be located during testing are measured and recorded prior to testing. These measurements are referred to as Personnel Exposure Limits (PEL) or more commonly Maximum Permissible Exposure (MPE) limits.

3.4 Maximum Permissible Exposure to Personnel

As discussed in Chapter 1, the presence of personnel is required to verify the operability of the system while being exposed to the environments defined in Tables 3.1 and 3.2. The exposure of personnel to these fields for extended durations can be hazardous. To ensure personnel safety, Maximum Permissible Exposure (MPE) limits are calculated in accordance with IEEE STD C95.1 (2005) "IEEE Standard for Safety Levels with Respect to Human Exposure to Radio Frequency Electromagnetic Fields, 3 kHz to 300 GHz" and Department of Defense Instruction (DODi) 6055.11 "Protecting Personnel from Electromagnetic Fields". A MPE is defined by DODi 6055.11 to be "the highest electric or magnetic strengths or power densities, or the induced and contact currents to which a person may be exposed without incurring an established adverse health effect and with an acceptable margin of safety".

Table 3.3. Maximum Permissible Exposures for Controlled RF Environments

Frequency range (MHz)	RMS electric field strength (E)[a] (V/m)	RMS magnetic field strength (H)[a] (A/m)	RMS power density (S) E-field, H-field (W/m^2)	Averaging time $|E|^2$, $|H|^2$ or S (min)
0.1–1.0	1842	$16.3/f_M$	$(9000, 100\,000/f_M^2)$[b]	6
1.0–30	$1842/f_M$	$16.3/f_M$	$(9000/f_M^2, 100\,000/f_M^2)$	6
30–100	61.4	$16.3/f_M$	$(10, 100\,000/f_M^2)$	6
100–300	61.4	0.163	10	6
300–3000	–	–	$f_M/30$	6
3000–30 000	–	–	100	$19.63/f_G^{1.079}$
30 000–300 000	–	–	100	$2.524/f_G^{0.476}$

NOTE—f_M is the frequency in MHz, f_G is the frequency in GHz.

[a]For exposures that are uniform over the dimensions of the body, such as certain far-field plane-wave exposures, the exposure field strengths and power densities are compared with the MPEs in the Table. For non-uniform exposures, the mean values of the exposure fields, as obtained by spatially averaging the squares of the field strengths or averaging the power densities over an area equivalent to the vertical cross section of the human body (projected area), or a smaller area depending on the frequency (see NOTES to Table 8 and Table 9 below), are compared with the MPEs in the Table.

[b]These plane-wave equivalent power density values are commonly used as a convenient comparison with MPEs at higher frequencies and are displayed on some instruments in use.

Figure 3.2. Non-ionizing Radiation: Selected Radio Frequency Exposure Limits

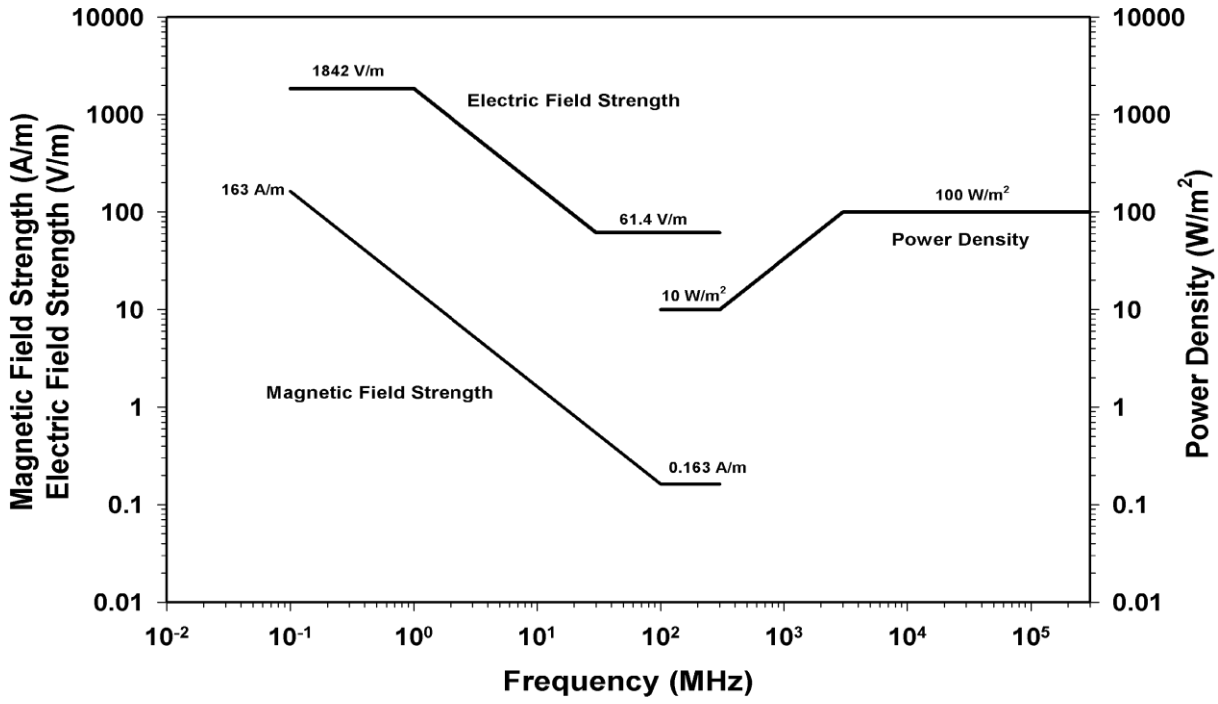

After the free field calibrations are performed the EUT (or helicopter) is moved into test position. MPE measurements are made by placing electric field probes in the location any pilot or crew member may be present during testing. Probes are positioned in a manner to capture the whole body average of test personnel. Typical probe positions are chosen at approximate heights of the head, chest, waist, and feet of personnel locations. The electric field probes are placed in this manner to capture a spatial average of the electric field where personnel will be located during testing. The electric field for each probe position is recorded and used to calculate the spatial average (from each set of four probes). The spatial average of the electric field probe measurements is calculated using a root mean square average to obtain a whole body average at each personnel location.

$$Spacial\ Average\ (V/m) = \sqrt{\frac{E_1^2 + E_2^2 + E_3^2 + E_4^2}{4}}$$

The whole body or spatial average is then used to calculate a MPE time limit for all specific test environments.

$$MPE\ Time\ Limit\ (secs) = \frac{Averaging\ Time\ (secs)}{((Spatial\ Average\ (V/m)^2)/(MPE\ (V/m)^2))}$$

The Averaging Time (secs) and MPE (V/m) can be found in Table 3.3. Figure 3.2 shows the MPE (V/m) limits in a graphical representation. During testing the MPE time limit is monitored by a test engineer to ensure the safety of the personnel being exposed to the high fields. The data presented in the following sections presents measured internal fields within different aviation platforms.

3.5 Measured Data

The data presented in this section were recorded while performing MPE measurements on the respective aviation platforms. All three platforms were subjected to EMV testing which

required personnel to be located inside the aircraft while being subjected to the high field environments. Only recorded data in which the measured internal field was greater than the free field calibration is presented in the following sections.

3.5.1 Boeing CH-47F Chinook

The Boeing CH-47 Chinook is an American twin-engine, tandem rotor heavy-lift helicopter. Its primary roles are troop movement, artillery placement and battlefield resupply. Its physical dimensions are shown in Figure 3.3 and Figure 3.4.

Figure 3.3. CH-47F Aircraft Height/Width Dimensions

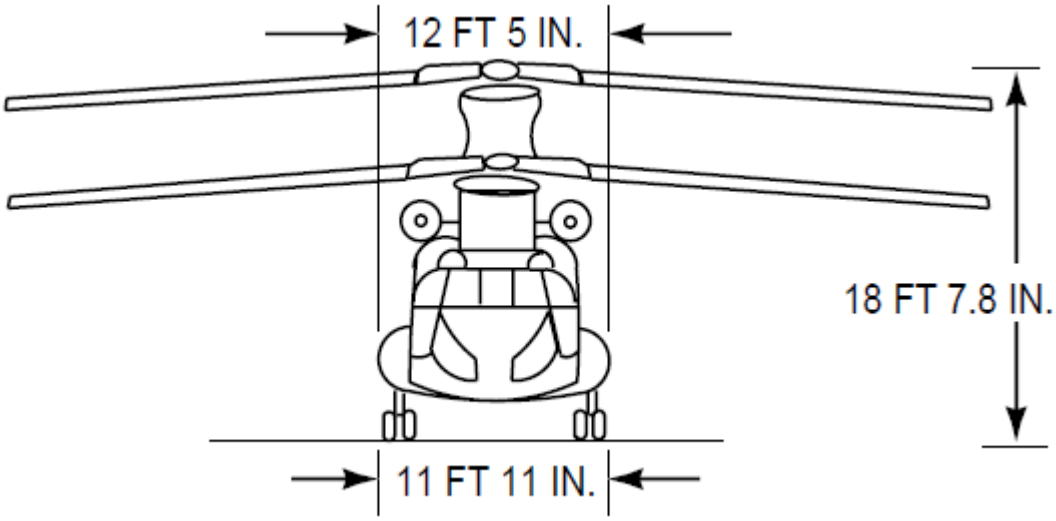

Figure 3.4. CH-47F Aircraft Length Dimensions

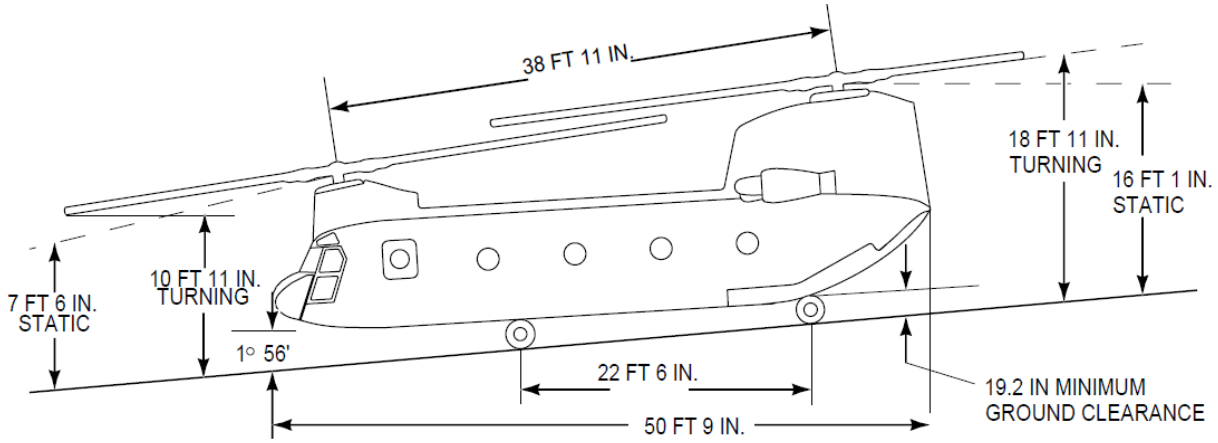

Figure 3.5 shows the antenna radiating positions during EMV testing and MPE measurements of the CH-47F. These positions were chosen due to the location of the equipment under test (EUT) and/or the radiating source. The electronics on this platform are primarily located in the cockpit, cabin avionics bays directly behind the pilot seats in the cabin and in the right side avionics bay. Countermeasure sensors are located towards the aft, fwd, and mid section of the aircraft. Engines and engine electronic controllers are located towards the aft of the aircraft. Antennas for navigation and communications are located at several positions on the aircraft. The antenna positions seen in Figure 3.5 were chosen to best immerse each EUT in the required field environments.

Figure 3.5. CH-47F 2011 Antenna Radiating Positions

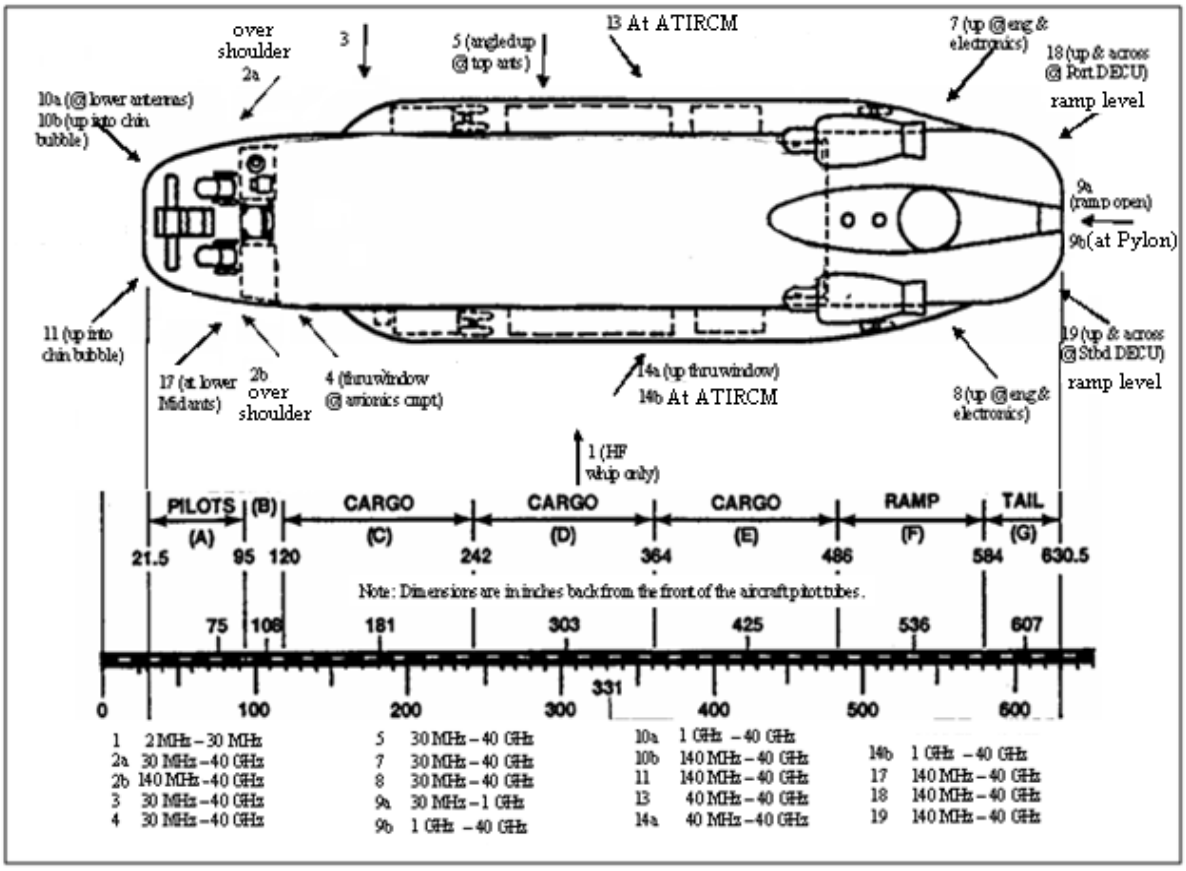

Tables 3.4 and 3.5 show instances where measured internal electric fields during MPE measurements were greater than the free field calibration. Measurements where there were no

readings above the calibrated field were omitted from the tables below. Also, for the purpose of this discussion, only frequencies below 1 GHz were considered. Table 3.4 shows the measured data for the cockpit area in the pilot and copilot locations. Table 3.5 shows the data for two crew positions located in the cabin of the aircraft. During testing, the crew members were restricted to these specific locations. Probe positions where the internal field exceeds the cal field are highlighted.

Table 3.4: CH-47F 2011 Measured Fields Greater than Cal Field (Cockpit)

Platform: CH-47F 2011				Left (Inside Cockpit)				Right (Inside Cockpit)			
Frequency (MHz)	Antenna Position	Antenna Polarization	Avg E-Field (V/m)	Probe 1	Probe 2	Probe 3	Probe 4	Probe 5	Probe 6	Probe 7	Probe 8
65	4	H	200	29.9	29	50.9	200.5	11.7	11.3	19.6	0
80	4	H	200	33.7	32.3	101.4	405.2	9.6	11.5	25.5	0
140	10b	H	200	24.5	31.4	31.6	75.1	51.7	68.8	43.9	268.3
140	2a	H	200	22.1	21.6	17.3	29.6	43.8	55.3	33.2	216.6
215	10b	H	200	54.4	71.6	63.9	47.9	59.1	63.4	21.4	208.8
235	10b	H	200	76.2	86.8	63.3	30	68.3	50.4	17.7	213.5
290	10b	H	200	45.6	42.2	33.8	28.9	68.4	115.6	14.1	302.6
390	10b	H	200	47.9	85.8	70.7	49	132.8	170.8	48.8	247.4
425	10b	H	200	53.5	53.7	49.3	67.3	114.7	122.5	127.3	357.4
425	11	H	200	239	146.5	127.2	288.9	98.5	69.2	20.3	23.4
450	11	H	200	124.6	178.2	117.6	306.1	132.7	89.6	36.7	30.9
450	10b	H	200	72.6	40.9	91.8	112.5	125	53.3	76.8	293.2
600	11	H	200	153.2	131.8	136.6	243.7	74.1	79	41.1	52
630	11	H	244	95.7	178.5	205.7	377.9	89.6	80.5	62.9	70
825	11	H	200	79.5	138.9	159	276.1	63.2	59.2	50.3	57.8
825	11	H	244	147.3	178.4	234.4	282.6	139	75	85.7	35.4
910	11	H	244	214.6	141.6	226.8	358	121.4	122.8	15.3	85.3
910	11	H	200	168	110.7	175.9	277.6	93.2	96	12.6	65.2
910	10b	H	244	63.7	45.3	76.5	67.2	99.5	135.4	166	314.3
910	10b	H	200	50.3	35.8	60.4	53.1	77.7	106.5	129.7	247.1
1000	11	H	200	121.6	106.5	100.3	369.5	98.7	38.7	55.5	34.5
1000	10b	H	200	83.5	72.2	52.1	57.5	194.3	125.4	218.8	184.9
140	10b	V	200	27.8	31	29.2	67.2	46.2	60.5	48	231.7
390	10b	V	200	62.3	60.8	54.1	45.6	82.3	101.2	28.8	216.9
425	11	V	200	140.1	107.1	105.4	272.5	44.9	104.7	68.9	49.9
425	10b	V	200	57.6	33.3	39.5	46.8	74.6	55.7	91.8	251.7
450	11	V	200	106.7	57.8	99.6	240.1	113.2	77.9	17.1	33.2

Platform: CH-47F 2011				Left (Inside Cockpit)				Right (Inside Cockpit)			
Frequency (MHz)	Antenna Position	Antenna Polarization	Avg E-Field (V/m)	Probe 1	Probe 2	Probe 3	Probe 4	Probe 5	Probe 6	Probe 7	Probe 8
600	11	V	200	122.7	149.3	142	234.7	110.7	45.2	15	38.2
630	11	V	244	197.6	146.1	83.4	299.3	97.6	76	20.7	46.3
910	11	V	244	281.6	164.4	121	143.4	111.8	138.4	74.9	86.4
910	11	V	200	228.9	133.1	98.5	119.5	89.7	112.5	59.7	68.8
1000	10b	V	200	108.1	98.1	110.7	67.1	185.8	168.3	95.9	221

Table 3.5: CH-47F 2011 Measured Fields Greater than Cal Field (Cabin Crew Area)

Platform: CH-47F 2011				Crew Position 1				Crew Position 2			
Frequency (MHz)	Antenna Position	Antenna Polarization	Avg E-Field (V/m)	Probe 9	Probe 10	Probe 11	Probe 12	Probe 13	Probe 14	Probe 15	Probe 16
80	9a	H	200	52.3	44.7	60.6	38.9	251.1	249.8	230.3	0
80	7	V	200	16.5	8.7	17.4	14.8	168.7	180.8	214.8	0
1000	18	V	200	27.8	27.2	18.7	40.4	172.1	152.4	211.2	98.8

It can be seen in Tables 3.4 and 3.5 there are several instances that the measured internal fields exceed the calibration field. These circumstances can be dangerous to personnel and limit exposure time. Figure 3.6 presents the data from Tables 3.4 and 3.5 in graphical form.

Figure 3.6. CH-47F 2011 Measured Fields Above Free Field Cal

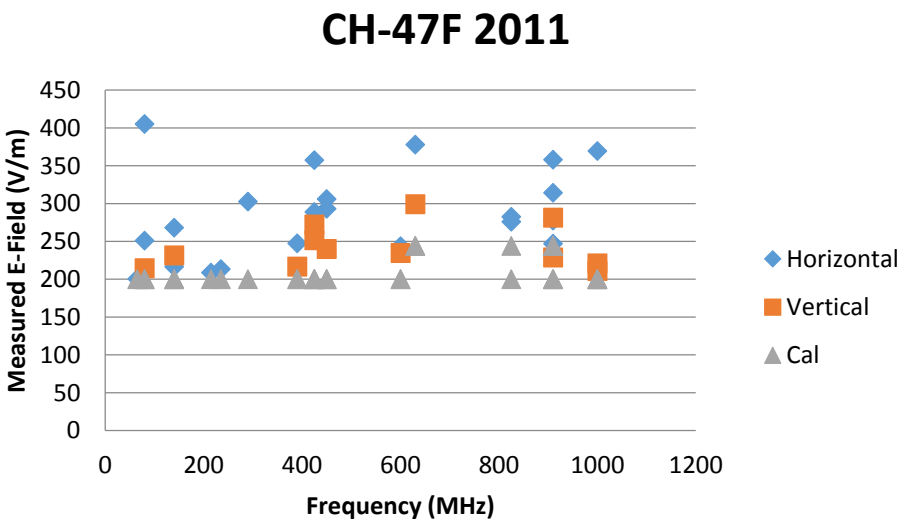

The highest probe reading was plotted for each field environment. It can be seen there are several instances where the measured field has been enhanced. These enhancements are as high as 200% at specific environments. This is a cause for concern due to personnel being exposed to these high fields during testing.

Additionally, test runs are often cut short prior to concluding due to MPE time limits. MPE time limits are calculated for each specific field environment using data collected during MPE measurements. Data presented in Table 3.4 was collected during MPE measurements on the CH-47F and can be used to calculate associated MPE time limits. An average of the electric field probe measurements is used to obtain a whole body average per personnel location. For the 80 MHz horizontally polarized field environment at position number four, the left cockpit location is the limiting position and will be used for the purpose of calculations. The spatial average of the left cockpit position can be determined by calculating the root mean square average of the four probe measurements at that location using the spatial average formula from Section 3.4.

$$Spacial\ Average\ (V/m) = \sqrt{\frac{33.7^2 + 32.3^2 + 101.4^2 + 405.2^2}{4}} = 210.148\ V/m$$

From Table 3.3, the averaging time and MPE limit (V/m) can be determined. For this specific case, the averaging time is equal to 360 seconds. The MPE limit is equal to 61.4 V/m at 80 MHz.

$$MPE\ Time\ Limit\ (secs) = \frac{360}{(\ 210.148^2)/(61.4^2)} = 30.7\ secs$$

The MPE time limit for the respective environment is equal to 31 seconds. Test runs durations are typically much greater than the MPE time limit. When the MPE time limit is reached the test run has to be cut short for a "cool down" period. The "cool down" period is equal to the averaging time minus the MPE time limit. For this case, the "cool down" period is equal to five

mines and 29 seconds. Typically, it takes several iterations to complete one full test run and consequently increase the duration of testing.

3.5.2 Boeing AH-64E Apache

The Boeing AH-64 Apache is a four-blade, twin-engine attack helicopter with a tandem cockpit for a two-man crew. Its physical dimensions are shown in Figure 3.7 and Figure 3.8.

Figure 3.7. AH-64D Height/Width Dimensions

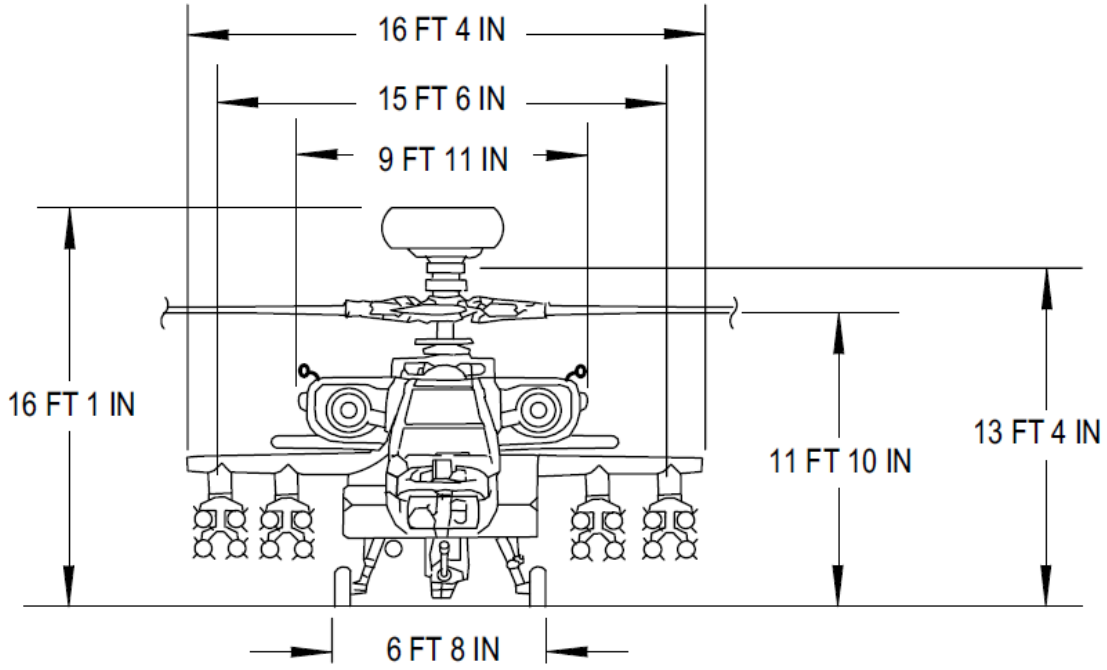

Figure 3.8. AH-64D Length Dimensions

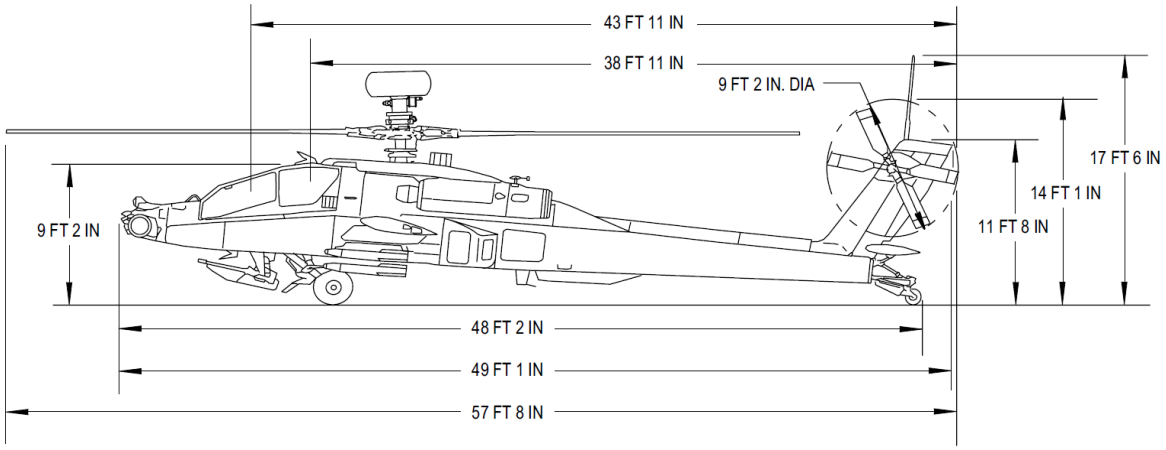

Figure 3.9 shows the antenna radiating positions during EMV testing and MPE measurements of the AH-64E. These positions were chosen due to the location of the equipment under test (EUT) and/or the radiating source. Electronics are located in the front avionics bays, transmission bays located under the wings and in the rear avionics bays. Weapon systems are located on the bottom on the aircraft underneath the front pilot and on each wing. Survivability sensors and antennas are located at several locations around the aircraft. The antenna positions seen in Figure 3.9 were chosen to best immerse each EUT in the required field environments

Figure 3.9. AH-64E 2012 Antenna Radiating Positions

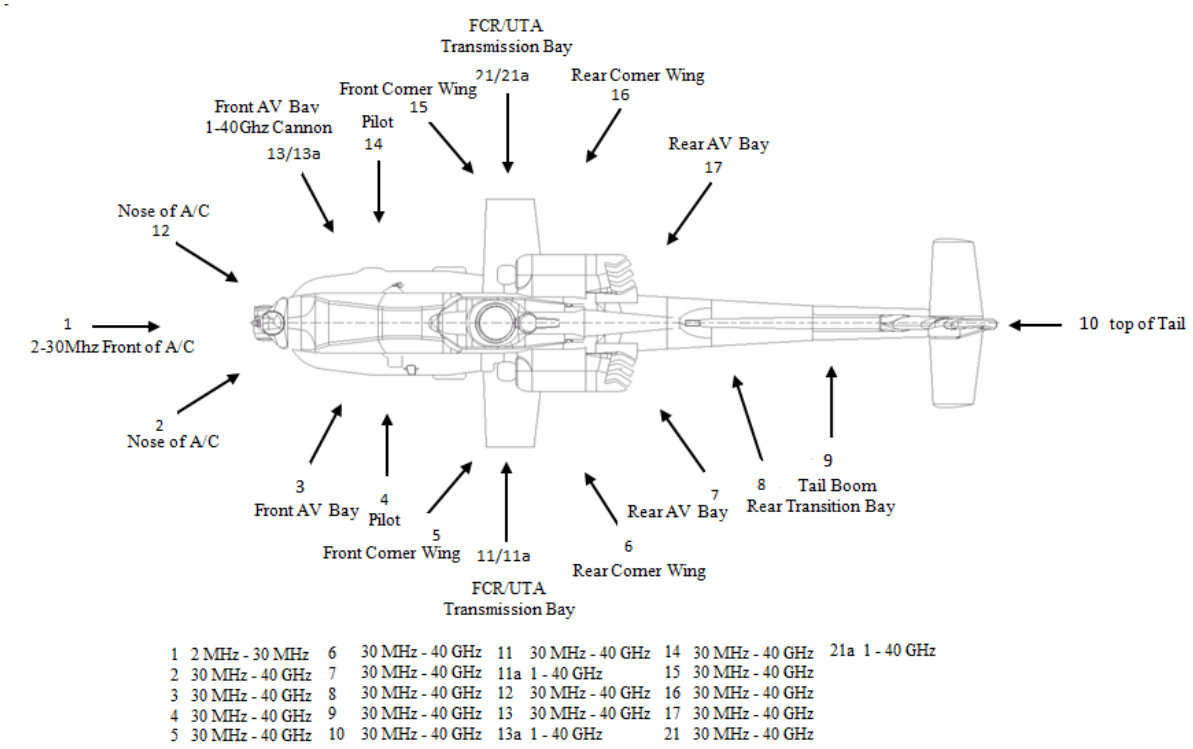

Table 3.6 shows instances where measured internal electric fields were greater than the free field calibration.

Table 3.6: AH-64E 2012 Measured Fields Greater than Cal Field

Platform: AH-64E 2012				Gunner Co-Pilot (Front Cockpit)				Pilot (Back Cockpit)			
Frequency (MHz)	Antenna Position	Antenna Polarization	Avg E-Field (V/m)	Probe 1	Probe 2	Probe 3	Probe 4	Probe 5	Probe 6	Probe 7	Probe 8
1000	14	H	200	211.9	87.4	78	30	266.7	145.7	82	37.3
1000	4	H	200	211.9	87.4	78	30	266.7	145.7	82	37.3
1000	14	V	200	185.6	93	92.9	41.5	201.7	115	84.7	22.9
1000	4	V	200	185.6	93	92.9	41.5	201.7	115	84.7	22.9

Figure 3.10. AH-64E 2012 Measured Fields Above Free Field Cal Plot

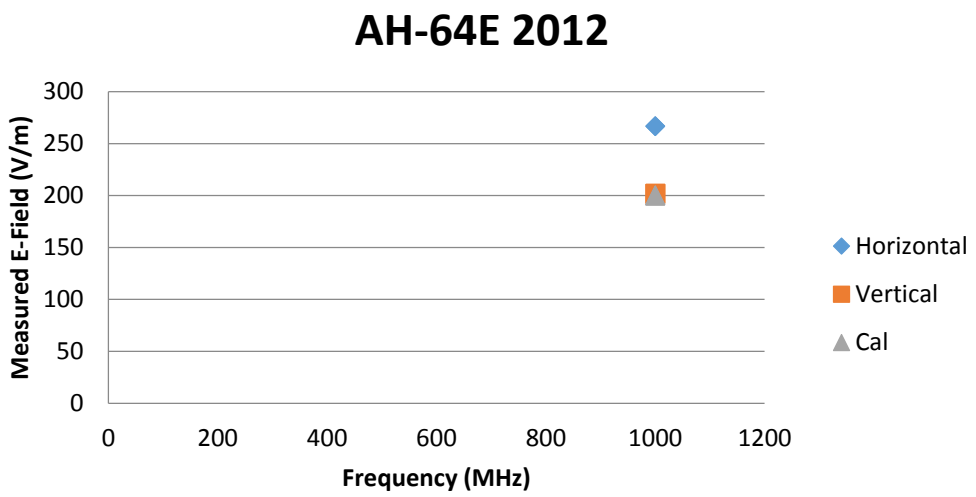

For this particular test no major enhancements were observed during MPE measurements. The only enhancement recorded was at 1 GHz were the field was approximately 132% of the calibration field.

3.5.3 Sikorsky UH-60L Black Hawk

The Sikorsky UH-60L Black Hawk is a four-bladed, twin-engine, medium lift utility helicopter. Its physical dimensions are shown in Figure 3.11 and 3.12.

Figure 3.11. UH-60A/L Height/Width Dimensions

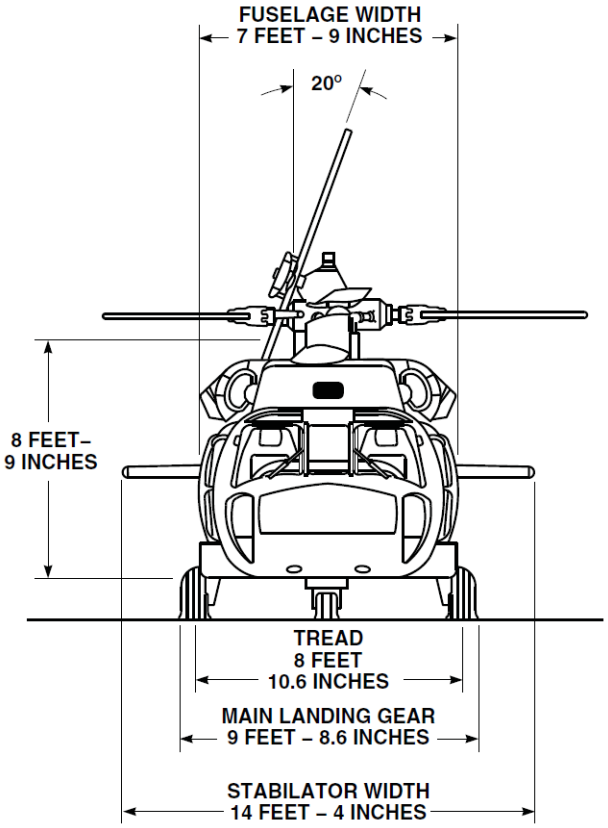

Figure 3.12. UH-60A/L Length Dimension

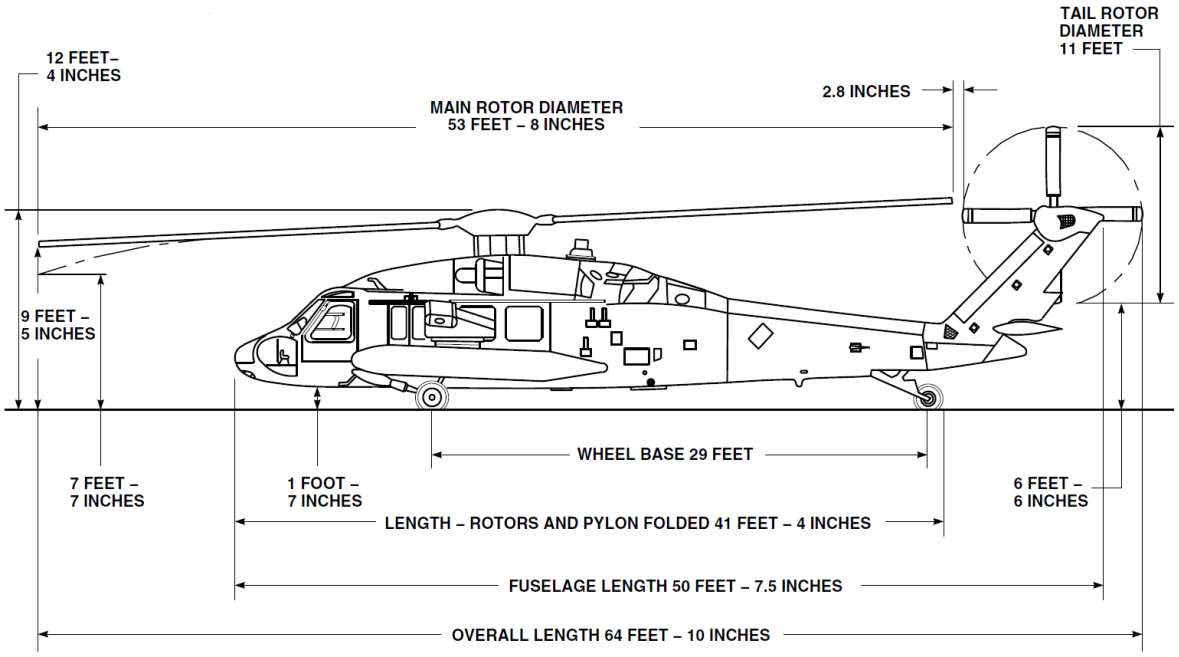

Figure 3.13 shows the antenna radiating positions during EMV testing and MPE measurements of the UH-60L. These positions were chosen due to the location of the equipment under test (EUT) and/or the radiating source. Avionics are primarily locked in the nose, cockpit and aft avionics bay. Sensors and antennas are located all around the skin of the helicopter.

Figure 3.13. UH-60L 2013 Antenna Radiating Positions

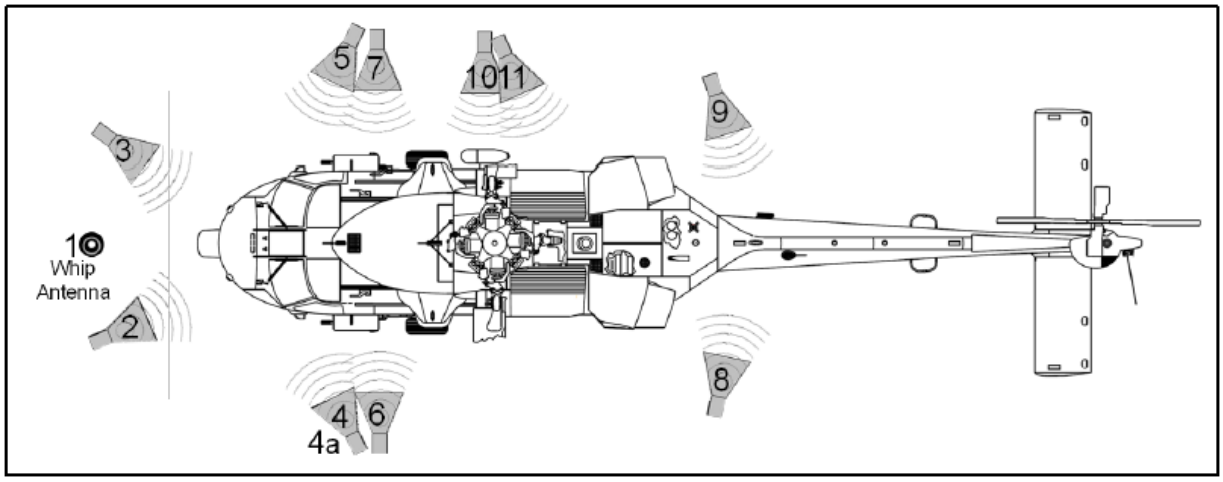

Table 3.7 shows instances where measured internal electric fields were greater than the free field calibration. No enhancements were seen in the cockpit area, therefore, that data was omitted from Table 3.7. There are several frequencies where the internal measured fields are greater than the calibration field.

Table 3.7: UH-60L 2013 Measured Fields Greater than Cal Field

Platform: UH-60L 2013				Crew Chief Station 1 (Right)			
Freq. (MHz)	Ant. Pos.	Ant. Pol.	Avg E-Field (V/m)	Probe 9	Probe 10	Probe 11	Probe 12
80	11	H	200	89.5	133.7	147.1	211.5
140	11	H	200	182.2	162.3	142.5	252.7
140	10	H	200	110.2	98.9	92.3	209.3
153.5	11	H	200	243.2	228.9	171.3	184.3
153.5	11	H	200	243.2	228.9	171.3	184.3
153.5	10	H	200	156.6	138.7	113.7	218.8
153.5	10	H	200	156.6	138.7	113.7	218.8
182	11	H	200	197	210.2	180.9	124.5
182	11	H	200	197	210.2	180.9	124.5

Platform: UH-60L 2013				Crew Chief Station 1 (Right)			
Freq. (MHz)	Ant. Pos.	Ant. Pol.	Avg E-Field (V/m)	Probe 9	Probe 10	Probe 11	Probe 12
215	11	H	200	407.2	451.5	289	166.5
215	11	H	200	407.2	451.5	289	166.5
215	11	H	200	407.2	451.5	289	166.5
215	10	H	200	301.8	362.8	220.8	189.6
215	10	H	200	301.8	362.8	220.8	189.6
215	10	H	200	301.8	362.8	220.8	189.6
223	11	H	200	429.6	518	286.2	174.9
223	11	H	200	429.6	518	286.2	174.9
223	10	H	200	283.8	347.4	170.2	206.7
223	10	H	200	283.8	347.4	170.2	206.7
235	11	H	200	401.9	431.1	231	87.9
235	11	H	200	401.9	431.1	231	87.9
235	11	H	200	401.9	431.1	231	87.9
235	10	H	200	202.6	239.9	140.6	197.3
235	10	H	200	202.6	239.9	140.6	197.3
235	10	H	200	202.6	239.9	140.6	197.3
290	11	H	200	207.4	133.2	79.6	148.8
290	11	H	200	207.4	133.2	79.6	148.8
290	11	H	200	207.4	133.2	79.6	148.8
325	11	H	200	291	203.1	124.4	119.2
325	11	H	200	291	203.1	124.4	119.2
325	11	H	200	291	203.1	124.4	119.2
325	10	H	200	144	210	142.2	57.5
325	10	H	200	144	210	142.2	57.5
325	10	H	200	144	210	142.2	57.5
390	11	H	200	217.5	144.4	125.2	98.8
390	11	H	200	217.5	144.4	125.2	98.8
390	11	H	200	217.5	144.4	125.2	98.8
450	11	H	200	226.7	129.7	160.9	88.4
450	11	H	200	226.7	129.7	160.9	88.4
450	11	H	200	226.7	129.7	160.9	88.4
630	11	H	244	286.7	234.2	289.1	256.6
630	11	H	200	225	185.1	228.8	199.3
630	11	H	200	225	185.1	228.8	199.3
153.5	11	V	200	169.1	157.8	125.7	305.8
153.5	11	V	200	169.1	157.8	125.7	305.8
182	11	V	200	114.5	117.4	102.8	216
182	11	V	200	114.5	117.4	102.8	216
215	11	V	200	243.4	288.3	209.8	366.9
215	11	V	200	243.4	288.3	209.8	366.9
215	11	V	200	243.4	288.3	209.8	366.9
223	11	V	200	213.2	248.3	161.3	283.7
223	11	V	200	213.2	248.3	161.3	283.7

Platform: UH-60L 2013				Crew Chief Station 1 (Right)			
Freq. (MHz)	Ant. Pos.	Ant. Pol.	Avg E-Field (V/m)	Probe 9	Probe 10	Probe 11	Probe 12
223	10	V	200	170.7	211.2	114.9	117.4
223	10	V	200	170.7	211.2	114.9	117.4
235	11	V	200	243.5	233	153.9	284.8
235	11	V	200	243.5	233	153.9	284.8
235	11	V	200	243.5	233	153.9	284.8
235	10	V	200	215.8	236.3	120.6	125.8
235	10	V	200	215.8	236.3	120.6	125.8
235	10	V	200	215.8	236.3	120.6	125.8
290	10	V	200	120.7	105.2	89.5	258.9
290	10	V	200	120.7	105.2	89.5	258.9
290	10	V	200	120.7	105.2	89.5	258.9
290	11	V	200	205.3	209.6	196.3	249.8
290	11	V	200	205.3	209.6	196.3	249.8
290	11	V	200	205.3	209.6	196.3	249.8
325	11	V	200	264	163	170.6	148
325	11	V	200	264	163	170.6	148
325	11	V	200	264	163	170.6	148
361	11	V	200	225	150.5	193.7	99.7
361	11	V	200	225	150.5	193.7	99.7
361	11	V	200	225	150.5	193.7	99.7
450	11	V	200	164.4	169.7	222.7	127.3
450	11	V	200	164.4	169.7	222.7	127.3
450	11	V	200	164.4	169.7	222.7	127.3

Figure 3.14 plots the highest probe reading at each of the environments from Table 3.7. The enhancements seen are as high as 250% for a specific horizontal field environment.

Figure 3.14. UH-60L 2013 Measured Fields Above Free Field Cal

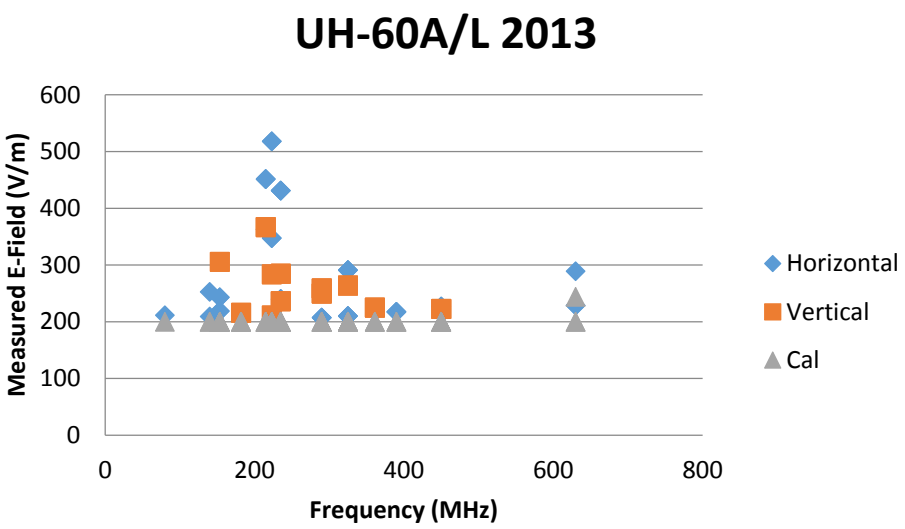

The data shown in Figure 3.14 can be compared to the data seen in Figures 2.2 and 2.3. The operating modes seen in the slotted circular cylindrical in Section 2.5.1 were: TE11-144 MHz, TE21-239 MHz, TE01-300 MHz, TE31-329 MHz, TM01-188 MHz, TM11-300 MHz and TM21-402 MHz. The slotted circular cylinder was designed to be a half size model representation of the Black Hawk helicopter. The operating modes for the Black Hawk helicopter ideally would be half those seen in the experiment. Therefore, the likely resonant frequencies would be expected to be in the range of half those seen in the controlled cylinder experiment: TE11-72 MHz, TE21-120 MHz, TE01-150 MHz, TE31-165 MHz, TM01-94 MHz, TM11-150 MHz and TM21-201 MHz. For both cases, the TE polarization was vertical and the TM polarization was horizontal. The data in Figure 3.14 is encouraging as the enhancements closely resemble the modeled and experimental data. There are variations, which were expected. Several factors could have attributed to the variances. First, the helicopter is not a perfect circular cylinder, nor is it hollow. Secondly, only discrete frequencies were tested that may not have aligned with the corresponding operating modes.

CHAPTER 4

CONCLUSIONS

This thesis explores the issue of high intensity electromagnetic fields inside the personnel areas (cockpit and cargo hold) of aviation platforms due to the internal resonances of these aircraft cavities. Experimental measurements were made using a slotted aluminum cylinder (7.62m length and 1.22m diameter) which was designed to be an approximate 1/2 scale representation of a Black Hawk helicopter fuselage. Models were also developed to calculate the resonant frequencies of the respective canonical slotted cylinder. Results from the models were then compared with the experimentally obtained measurements made internal to the aluminum scale model. The correlation between the two sets of data (computation predictions vs measured fields) was encouraging. It was seen, at the predicted resonant frequencies of the cylinder, the fields measured inside were greatly intensified, as the computed models suggested would obtain.

Further data was collected and analyzed from measurements on various aviation platforms as a natural consequence of preparing for required EMV testing of helicopter platforms. Measured electric fields greater than the cal field were observed inside of each of the three platforms discussed during this thesis. There was a strong correlation between the modeled and experimental data to the data that was measured on the actual Black Hawk helicopter. Several factors contribute to these obvious variances. Although the interior cockpit and cargo hold geometries are naturally of complicated geometry, there still exists the potential for

resonance phenomena in the natural cavities. The potential for increased fields due to resonant frequencies was again observed repeatedly in real aircraft platforms.

The potential for internal resonances to produce extremely high electromagnetic fields internal to the different platforms is a cause for concern due to the presence of personnel during EMV testing. Over exposure to fields greater than the maximum permissible exposure limits can be a potential health risk to the subjected individual. Over time, without the proper monitoring, the body temperature will begin to rise and has the potential to cause damage. It is imperative that the potential for increased internal fields not be ignored during testing. Measurements and proper monitoring of personnel exposure limits is required to ensure the safety of all involved.

REFERENCES

[1] Waller, M. L. and T. H. Shumpert, "Comparison of Measured vs. Modeled TE and TM Field Penetration into a Slotted Circular Cylinder," IEEE Progress in Electromagnetics Research B, Vol 28, 201-218, 2011.

[2] Shumpert, T. H., M. L. Waller, S. H. Wong, and R. W. Scharstein, " Coupling Issues Associated with Electromagnetic Vulnerability (EMV) Testing of Vehicles Over Groud," IEE Progress in Electromagnetics Research, Vol. 124, 457-471, 201.

[3] Pozar, David M., *Microwave Engineering, Third Edition.* John Wiley and Sons, 2005.

[4] Wentworth, Stuart M., *Applied Electromagnetics: Early Transmission Lines Approach.* John Wiley and Sons, 2007.

[5] Chu, L. J., "Chapter 6: Metallic Waveguide and Cavity Resonators".

[6] *Electromagnetic Enviornmental Effects Requirements for Systems*, Department of Defense Standard Interface Standard, MIL-STD-464C, 1 December 2010.

[7] *Electromagnetic Enviornmental Effects (E3) Performance and Verification Requirements,* Aeronautical Design Standard, ADS-37A-PRF, May 28, 1996.

[8] *IEEE Standard for Safety Levels with Respect to Human Exposure to Radio Frequency Electromagnetic Fields, 3 kHz to 300 GHz,* Institute of Electrical and Electronics Engineers (IEEE), IEEE Std C95.1-2005, 19 April 2006.

[9] *Protecting Personnel from Electromagnetic Fields,* Department of Defense Instruction, Number 6055.11, 19 August 2009.

[10] Waller, M. L., "Personnel Exposure Limits for EMRO Testing". April 5, 2006.

[11] *Waveguide Advantages,* http://electriciantraining.tpub.com, 10 February 2014.